8

Oxygen Isotope Exchange in Nanocrystal Oxides

Anatoly Fishman[1], Tatyana Kurennykh[2], Vladimir Vykhodets[2] and Evgeniya Vykhodets[3]
[1]*Institute of Metallurgy, Ural Division, Russian Academy of Sciences,*
[2]*Institute of Metal Physics, Ural Division, Russian Academy of Sciences,*
[3]*Ural Federal University, Yekaterinburg*
Russia

1. Introduction

The subject of investigation in this work is oxygen isotope exchange (OIE) between oxides and oxygen-containing gases $^{18}O_2$ and $C^{18}O_2$. OIE studies yield information about the rate of processes on the gas – solid interface and oxygen self-diffusion in oxides. In turn, the surface processes can involve some elementary stages, in particular, physical and chemical adsorption. Several types of diffusion processes can be observed also inside oxides, for example, volume and grain boundary diffusion. OIE investigations are of much practical interest, for example, in connection with the problems of catalytic oxidation of metals and development of materials for chemical and electrochemical devices (fuel cells, electrolyzers, sensors, hydrogen storage devices, devices for separation of gas and isotope mixtures, etc.).
Two experimental approaches to OIE examination are known. The pioneer approach was based on measurements of the isotope composition of a gas mixture interacting with oxide. In the alternative approach developed in the last decades, the isotope composition of the oxygen subsystem of oxides was measured, which was studied usually by secondary ion mass spectrometry (SIMS) and nuclear microanalysis (NRA). The present work is devoted to the examination of the isotope composition of solid-state samples. The overwhelming majority of studies by means of this approach were performed on bulk samples. A distinguishing feature of this work is its orientation toward isotope exchange examination in nanoscale oxides. As will be shown below, this results in novel or supplementary data on the surface reaction rates during isotope exchange and the rates of diffusion processes in oxides. Moreover, the investigations into oxygen isotope exchange in oxide nanomaterials are of great practical importance. It is not improbable that the use of nanomaterials may lead to favorable changes in the functional properties of oxides when it is necessary to increase the quantity of absorbed gas or to increase rates of gas absorption or extraction etc.

2. Investigations on bulk samples

Most often, OIE studies on bulk samples involve isothermal annealing of samples in oxygen (or other oxygen-containing gas) enriched with ^{18}O isotope and measurement of

concentration profiles (depth distribution) of ^{18}O tracers in the sample. In case of bulk diffusion described by one value of oxygen self-diffusion coefficient D, the concentration profile $C(x,t)$ is described by the expression (Ruiz & Kilner, 1997)

$$C(x,t) - C_G = C_S^{\max}\left[erfc\,(Z) - \exp\left(Hx + H^2Dt\right) erfc\left(Z + \frac{Hx}{2Z}\right)\right],\ Z = \frac{x}{2\sqrt{Dt}}, \quad (1)$$

where H is a parameter characterizing the surface energy barrier; $C_S^{\max}$ is the maximal permissible concentration of ^{18}O atoms on the surface of a sample; t is the diffusion annealing time; C_G is the concentration of ^{18}O in a sample prior to annealing. According to (Ruiz & Kilner, 1997), the parameter H in expression (1) is connected with the parameter k characterizing the surface reaction rate during isotope exchange by the relation

$$k = HD\,. \quad (2)$$

It is seen from expressions (1)-(2) that OIE studies on bulk samples provide measurements both of diffusion coefficients D and surface reaction rates k.

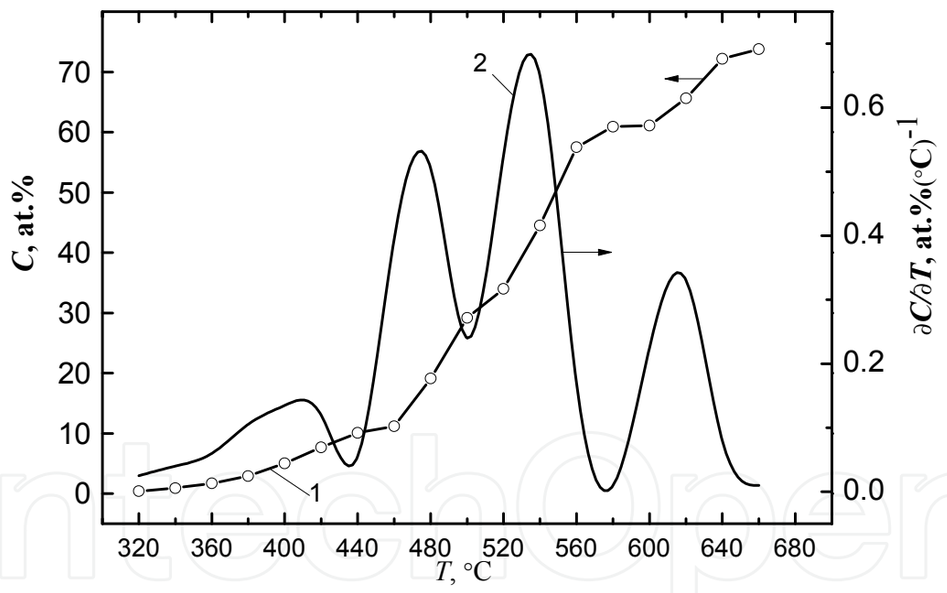

Fig. 1. Temperature dependence of concentration C and derivative $\partial C/\partial T$ during step-wise isochronous annealing of $YBa_2Cu_3O_{7-\delta}$ (Vykhodets et al., 1994). The concentration is given in percents of the number of positions in the oxygen sublattice of the oxide

For strongly anisotropic diffusion systems (HTSC oxides and other oxides with complicated crystal structure and chemical composition), a different route of OIE experiments can be chosen. In some works, step-wise isochronous annealing of samples was carried out in oxygen enriched with ^{18}O isotopes. The isochronous annealing conditions can be selected such that the systems with strong anisotropy of oxygen diffusion coefficients can exhibit a

site-plane effect. It consists in successive substitution of ^{18}O atoms for crystallographic oxygen planes or positions occupied by ^{16}O atoms before annealing.
By way of example, Fig. 1 demonstrates the isochronous-annealing curve $C(T)$ and its derivative $\partial C/\partial T$ characterizing the variation in ^{18}O isotope concentration C in $YBa_2Cu_3O_{7-\delta}$ samples as a function of experiment temperature T (Vykhodets et al., 1994). The results displayed in Fig. 1 show that there are several types of energetically non-equivalent sites for oxygen atoms in the oxide lattice.
The data on the site -plane effect make it possible to obtain information about the fraction of each type of sites in the oxygen subsystem of the oxide, to estimate the activation energy and the frequency factor for oxygen atom transition from one site to another, as well as to examine the effect of phase transformations in oxides on the distribution of oxygen atoms in the lattice sites, etc.

3. Investigations on nanocrystalline powders

The concentration profiles of ^{18}O atoms in a nanoparticle can not be determined experimentally since neither SIMS nor NRA methods ensure the locality of measurements commensurable with the size of nanopowder particles. Therefore, in our OIE studies on nanopowders we measured the average concentration of ^{18}O atoms in a large assembly of powder particles (Gizhevskii et al, 2008); the same assembly was annealed in oxygen enriched with ^{18}O isotopes. In view of the destructive character of SIMS measurements, this technique can scarcely be used to determine the average oxygen isotope concentration in powders. Here, the NRA method, which permits measurement of ^{18}O and ^{16}O atom concentration in the depth to several microns without sample failure, is certainly advantageous.
At first, we shall consider the isotope exchange model, in which only oxygen ions from the external atomic layer of the oxide particle participate. Let only $^{18}O_2$ molecules be present in the gaseous phase, while the oxide particle contains no ^{18}O atoms at all in the start time. In that case, the differential equation for isotope exchange has the form

$$dN_{18} = N_{16}\Gamma dt \quad , \tag{3}$$

where dN_{18} is the number of ^{18}O atoms that entered into the oxide during time dt; N_{16} is the number of ^{16}O atoms located in the instant time t on the surface of the oxide atomic layer; Γ is the frequency, with which ^{16}O atom in the oxide surface atomic layer is replaced by ^{18}O atom. Generally, this parameter is a function of the annealing temperature and the pressure in the gaseous phase. During isotope exchange, when neither oxidation nor reduction of the oxide take place, for the numbers of atoms ^{16}O and ^{18}O the relation $N_{16} + N_{18} = \text{const}$ is fulfilled. Then equation (3) for spherical particles is solved as

$$C(t) = C_0 \frac{3\Delta}{r}\left(1 - \exp(-\Gamma t)\right) \quad , \tag{4}$$

where $C(t)$ is the average concentration of ^{18}O atoms in the oxide; Δ is the monolayer thickness in the oxide; r is the particle radius; C_0 is the atomic concentration of oxygen in the oxide. For arbitrarily shaped particles it is easy to obtain an analogous "relaxation"-type dependence

$$C(t) = C_0 S\rho\Delta\left(1-\exp(-\Gamma t)\right) \ , \tag{5}$$

where S is the powder specific surface determined usually with the BET technique and ρ is the oxide density. Frequency Γ measured in OIE experiments on oxide powders is an analogue of the parameter k in formula (2). Based on the results (Vykhodets et al., 2000), it is possible to establish a correlation between Γ and k

$$k = l\Gamma \ , \tag{6}$$

where l is an atomic jump distance.

A fundamentally different "diffusion" model for the description of OIE (Gizhevskii et al, 2008) is used for processes characterized by the very high surface reaction rate and by comparatively slow volume diffusion of oxygen in the oxide particle. Here, for spherically shaped particles it is easy to obtain

$$C(t) = C_0\left(1-\frac{3\Delta}{r}\right)\left(1-\frac{6}{\pi^2}\sum_{s=1}^{\infty}\frac{1}{s^2}\exp\left(-\left(\frac{s\pi}{r}\right)^2 Dt\right)\right)+C_0\frac{3\Delta}{r} \quad . \tag{7}$$

Finally, the OIE model version providing for simultaneous implementation of the relaxation and diffusion mechanisms (Gizhevskii et al, 2008) was considered. In this case, the $C(t)$ dependence is found by numerical calculations.

Expressions for relaxation-type isotope exchange analogous with (4)-(5) will be valid not only at very slow oxygen diffusion in oxide, when a typical diffusion length is $(Dt)^{1/2} < d$ (d is the oxide particle size). It can be shown (Fishman et al, 2009) that they are correct also at very fast diffusion when $(Dt)^{1/2} \gg d$. In that case, all oxygen ions of the oxide particle take part in isotope exchange, and the concentration of ^{18}O atoms becomes similar in the bulk of the particle more quickly than it grows on the boundary with the gaseous phase. Here we have

$$C(t) = C_0\left[1-\exp\{-(3\Delta/r)\Gamma t\}\right] \tag{8}$$

or

$$C(t) = C_0\left[1-\exp\{-(S\rho\Delta)\Gamma t\}\right] \ . \tag{9}$$

From the aforesaid it is seen that the examination of isotope exchange on nanopowders may give data on their dimensional characteristics. Otherwise, the information received from isotope exchange studies on powders and bulk samples is in many respects analogous. This concerns both the diffusion characteristics of oxide materials and the processes on the surface of oxides.

OIE studies on nanopowders attract particular interest since they permit measuring low D values. Analysis of expression (7) shows that diffusion coefficients of oxygen tracers as small as 10^{-23} - 10^{-24} m^2/s or ever lower can be measured in such studies. This level of measurements is due to the small size of the powder nanoparticles, and is not typical of OIE investigations on bulk samples.

Expressions (4),(7),(8) are written for spherically shaped particles with a single value of the particle radius r. Certainly, for real powders, dimension distribution of powder particles

should be taken in account (Fishman et al, 2009). Corresponding relaxation-type dependences for an assembly of different-size particles can be easily obtained. For example, for $(Dt)^{1/2} \ll d$ we have

$$C(t) = C_0 3\Delta\left[1 - \exp\{-\Gamma t\}\right]\sum_i r_i^2 \Big/ \sum_i r_i^3 \quad , \tag{10}$$

and for $(Dt)^{1/2} \gg d$

$$C(t) = C_0 \sum_i r_i^3 \left[1\text{-}\exp\{\text{-}(3\Delta / r_i)\Gamma t\}\right] \Big/ \sum_i r_i^3 \quad . \tag{11}$$

The expediency and informativity of experimental studies of isotope exchange on nanopowders is not a trivial problem. First, there may be an unacceptable diversity of annealing conditions for individual particles contained in the powder assembly. Agglomeration of powders aggravates the situation. Second, analysis of expressions (10)-(11) shows that the presence in a nanopowder of large, for example, micron-size particles will result in a very strong decrease in the ^{18}O concentration as compared with that for a powder containing no large particles. Even with a small part of large particles, isotope exchange experiments may turn out senseless since the experimental data on $C(t)$ will characterize to a greater extent the isotope exchange on large particles rather than the assembly of particles. Virtually, this means that the considered technique will be effective only for nanopowders with a narrow size distribution function of powder particles.

Taking into consideration the above observations, in this work we devote much attention to the optimization of the technique for experimental studies on nanopowders, in particular, we examine powders obtained by different technologies and analyze the quantitative correspondence between the theoretical and experimental $C(t)$ values.

4. Oxygen isotope exchange with oxide powders

In this work we present OIE data for oxide nanopowders produced by mechanoactivation (grinding), laser sputtering of a ceramic target, and electrical explosion of wire. In some cases, comparative studies on micropowders were also performed. These technologies are characterized by the following features. The powders obtained by laser sputtering of a ceramic target or by electrical explosion of wire are traditional nanopowders with particles ranging within the nanoscale interval. For the nanopowders produced by grinding, the term *nanopowder* is not conventional. The size of their particles is usually within the micron range. At the same time, such powders have also nanoscale characteristics: the average size of X-ray coherent scattering domains is often of the order of 10 nm.

4.1 Oxygen isotope exchange with oxide powders $LaMnO_{3+\delta}$

The oxide $LaMnO_{3+\delta}$ is a convenient model object for optimization of the OIE technique (Gizhevskii et al, 2008) on nanopowders. In practice, there often occurs uncontrolled doping and diffusion characteristics of oxides are known to be extremely sensitive to the presents of impurities. Naturally, such materials are difficult to be analyzed. At the same time, nonisovalent doping of the cationic sublattice of $LaMnO_{3+\delta}$ does not lead to the formation of structural vacancies in the oxygen sublattice and oxygen volume diffusion coefficients

change only slightly in this oxide (Fishman et al., 2003). Probably, this effect is connected to variable valence of manganese ions (Mn^{2+}, Mn^{3+}, Mn^{4+}).

The micropowder $LaMnO_{3+\delta}$ was synthesized by the standard ceramic technology from oxides La_2O_3 and Mn_3O_4. A single-phase manganite powder with the orthorhombic crystal lattice and the particle size of about several microns was obtained. A FRITSCH planetary ball monomill was used to produce a nanostructured material from the initial powder. The grinding was in air in ethyl alcohol. Zirconium dioxide grinding balls and cups were used. The time of grinding was 13 h. According to X-ray diffraction results, the ground powder had an orthorhombic modification with the average coherent scattering domains of about 15 nm.

Isothermal annealings of nano- and micropowders were carried out in oxygen enriched by 80% with ^{18}O isotope. Oxygen pressure was 0.26 atm. The change in the isotope composition of the gaseous atmosphere during annealing was negligible. Previously, stabilization annealings of the powders had been performed in air at the same temperatures as in oxygen containing tracer atoms. Their duration was approximately the same as the maximal time of annealing in $^{18}O_2$. The annealings were carried out in a quartz tube. The temperature of samples was measured with a chromel-alumel thermocouple with an accuracy of 2°C.

The concentration of ^{18}O in the samples was determined with NRA using a 2 MV Van de Graaff accelerator (reaction $^{18}O(p, \alpha)^{15}N$), the incident beam energy being 762 keV. The sample plane surface was mounted perpendicular to the incident beam axis. The acceptance angle of the nuclear reaction products was 160°. The energy spectra of the reaction products were registered with a silicon surface barrier detector of 10 mm in diameter. The diameter of the primary proton beam was from 1 to 2 mm. The number of incident beam particles reaching the sample was measured with an accuracy of ~1% using a secondary monitor. For control by means of reaction $^{16}O(d, p)^{17}O^*$ when the incident beam particle energy is 900 keV, the content of ^{16}O isotopes in samples was measured. The total oxygen concentration in all the samples was the same to within several percents.

The concentration of ^{18}O and ^{16}O isotopes was measured immediately on powders. For this purpose, the powder particles were pressed into a plate of indium. As a result, a layer containing only particles of oxide with thickness large than 2 μm was formed on the plate of indium. Nondestructive analysis by means of the NRA technique was performed to the depth of about 2 μm. In the test experiments the spectra of reaction products $^{16}O(d, p)^{17}O^*$ and $^{18}O(p, \alpha)^{15}N$ for a bulk oxide and for powders, which were not annealed in the atmosphere of tracer atoms, did not differ within experimental error. The concentration profiles were calculated using the stopping power data for the examined samples (Vykhodets et al., 1987).

Experimental and calculated $C(t)$ dependences for the ground powder $LaMnO_{3+\delta}$ are given in Fig. 2. In our model calculations we considered several OIE scenarios for systems with low oxygen volume diffusion coefficients. In particular, the experimental data were processed using relaxation (4) and diffusion (7) expressions, as well as different powder particle size distribution functions. We also considered models for simultaneous realization of relaxation and diffusion mechanisms. For numerical calculations, corrections were introduced to expressions (4) and (7), which are due to the experimental conditions: presence of ^{18}O atoms in powders before annealing and value of gas enrichment with ^{18}O atoms. A similar correction of theoretical expressions for $C(t)$ was made while processing the experimental data for other oxides.

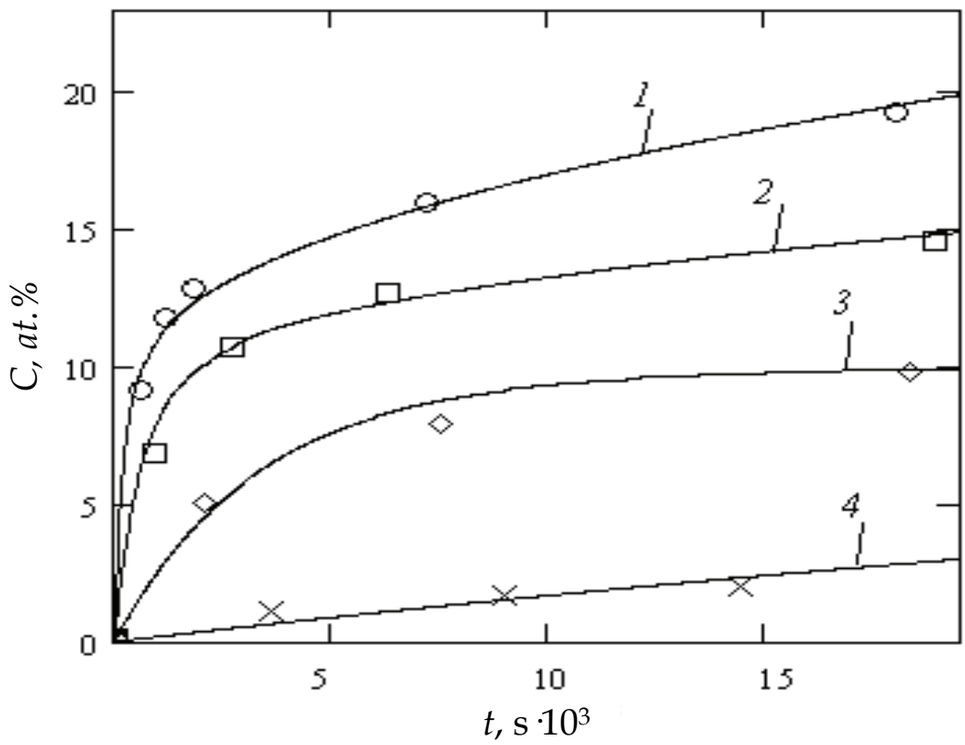

Fig. 2. $C(t)$ dependences for ground powder $LaMnO_{3+\delta}$ (Gizhevskii et al, 2008): 1 – 560^{0}C; 2 – 500^{0}C; 3 – 400^{0}C; 4 – 300^{0}C. Dots – experimental data; lines – calculation in the model for simultaneous realization of relaxation and diffusion mechanisms. Calculated curve parameters: 560^{0}C - $\Gamma = 5.17 \cdot 10^{-3}$ s^{-1}, $D = 1.35 \cdot 10^{-23}$ m^2/s; 500^{0}C - $\Gamma = 1.70 \cdot 10^{-3}$ s^{-1}, $D = 3.55 \cdot 10^{-24}$ m^2/s; 400^{0}C - $\Gamma = 3.07 \cdot 10^{-4}$ s^{-1}; 300^{0}C - $\Gamma = 1.93 \cdot 10^{-5}$ s^{-1}. At 400 and 300^{0}C, the diffusion contribution to the calculated dependences was negligibly small. In the calculations, r = 7.5 nm and Δ = 0.5 nm were assumed

It turned out that the experimental dependences $C(t)$ are not described in terms of diffusion theoretical models assuming no surface energy barrier during isotope exchange. In relaxation models, satisfactory fit with experimental data was shown only for low temperatures (300 and 400^{0}C). For elevated temperatures (500 and 560^{0}C), the best fit with experimental data was achieved in the model for simultaneous relaxation and diffusion. The caption to Fig. 2 contains the values of isotope exchange frequencies Γ and oxygen volume diffusion coefficients D, which provide satisfactory fit with experimental dependences $C(t)$. The temperature dependence of frequency Γ (see Fig. 7) can be described with the Arrhenius expression for the frequency factor $\Gamma_0 = (0.97 \cdot 10^3 \pm 0.70 \cdot 10^3)$ s^{-1} and the activation energy E = (0.88±0.07) eV.

The results presented in Fig. 2 showed that the technique for OIE examination on oxide nanopowders proposed in work (Gizhevskii et al, 2008) is consistent. It furnishes information about nanopowder dimensional characteristics, reaction rates on the oxide particles surface during isotope exchange, and oxygen volume diffusion coefficients in oxides. The reliability of the technique is supported by the following facts. The best possible

fit with the experimental dependences $C(t)$ was provided by the nanoparticle radius r = 7.5 nm, which is close to the experimentally determined average radius of the X-ray coherent scattering domain for the examined powder (6.5 nm). Thus, the main dimensional parameter of the powder responsible for the isotope exchange rate became apparent, namely, the size of the X-ray coherent scattering domains. The difference between 6.5 and 7.5 nm is not fundamental since the notion of the monolayer thickness is not strictly defined; in fact, it is a parameter of theory. The value Δ = 0.5 nm was assumed by the authors merely by tradition. For example, in the grain boundary diffusion studies, exactly this value was postulated for the grain boundary width. The oxygen volume diffusion coefficients (see caption to Fig. 2) obtained from $C(t)$ dependences processing also proved to be quite reasonable. For strontium-doped $LaMnO_3$–based perovskites, experimental oxygen volume diffusion coefficients are available in the literature for higher temperatures (Carter et al. 1992; De Souza et al. 2000; Fishman et al., 2003; Routbort et al., 1997). Strontium was not found to have any profound effect on the volume diffusion coefficients of tracer oxygen atoms (Fishman et al., 2003). Extrapolated diffusion coefficient values ranged from $1 \cdot 10^{-24}$ to $6 \cdot 10^{-24}$ m^2/s (for 500^{0}C) and from $1.6 \cdot 10^{-22}$ to $3.2 \cdot 10^{-23}$ m^2/s (for 560^{0}C) (see Fig.5). The values obtained in this work (see Fig. 5 and caption to Fig. 2) are within the above-mentioned intervals.

From Fig. 2 it is seen that the calculated and experimental dependences $C(t)$ agree to a high accuracy. This finding is important in two respects. First, it reveals that the size distribution function of powder particle was rather narrow when the grinding technology was used. Second, it shows that the differences in annealing conditions in $^{18}O_2$ for individual particles contained in the powder assembly were insignificant. Therefore, the same technology was applied in experiments with other powders.

From general considerations it was obvious that the value of frequency Γ should depend on the oxide type and the kind of oxygen-containing molecules in the gaseous phase. For the theoretical parameter Δ, the presence or absence of such dependence is not trivial. Therefore, we compared OIE kinetics for $LaMnO_{3+\delta}$ nanopowders annealed in $^{18}O_2$ and $C^{18}O_2$. The degree of carbon dioxide enrichment with ^{18}O isotopes was 90%; the pressures of oxygen and carbon dioxide during annealing were similar. The $C(t)$ data for 400^{0}C obtained during annealing in $C^{18}O_2$ were satisfactorily described by expression (4), while the concentrations of ^{18}O isotopes in the powder were from 1.5 to 2 times higher than those in oxygen. It was also found that the values of Γ and Δ increased when $^{18}O_2$ was replaced by $C^{18}O_2$. The corresponding values were $3.07 \cdot 10^{-4}$ and $6.4 \cdot 10^{-4}$ s^{-1} for Γ and 0.5 and 0.66 nm for Δ. The question why the surface layer thickness Δ varies when the kind of the oxygen-containing molecule of the gaseous phase is changed calls for further research.

Figure 3 demonstrates experimental $C(t)$ dependences for $LaMnO_{3+\delta}$ micropowder. They do not differ qualitatively from those for the nanopowder (Fig. 2) and can be also used to receive the information about surface reaction rates and oxygen diffusion coefficients in oxide. It is seen from comparison of the data in Figs. 2 and 3 that the dimensional factor showed up very vividly: the concentrations of ^{18}O isotopes in the micropowder were tens times lower. Evidently, the $C(t)$ dependences for nanopowders are more convenient for theoretical analysis than the data for mircopowders. In case of nanopowders, a better accuracy of analysis results is achieved. Besides, for microparticles, the particle spherical shape approximation and, consequently, the self-diffusion equation may turn out unsatisfactory.

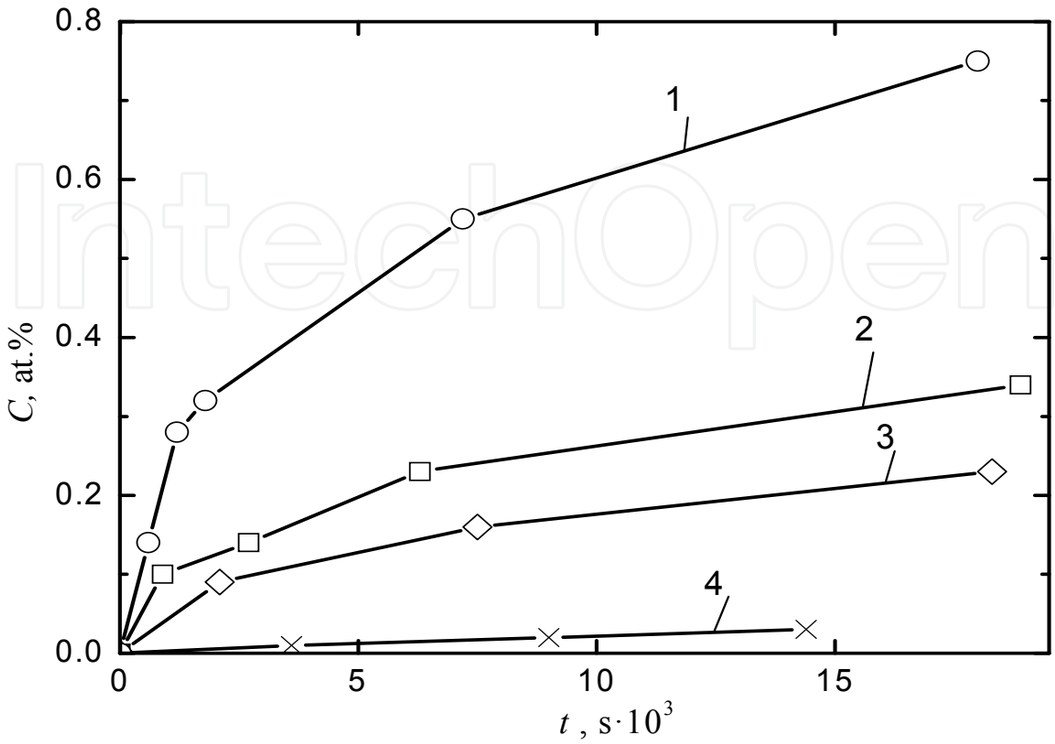

Fig. 3. Experimental dependences $C(t)$ for $LaMnO_{3+\delta}$ micropowder: 1 – 560^{0}C; 2 – 500^{0}C; 3 – 400^{0}C; 4 – 300^{0}C

4.2 Oxygen isotope exchange with α-Mn_2O_3 oxide powders

Manganese oxides are technically important and scientifically interesting materials. However, for these species, as far as we know, there is no information about OIE, oxygen diffusion coefficients, and surface reaction rates in the interaction with gaseous oxygen. Therefore, in this work we carried out appropriate studies on α-Mn_2O_3 oxide powders produced by mechanoactivation.

A planetary mill AGO-2 was used to prepare Mn_2O_3 powders. Nanoscale domains were formed for a much shorter period of time than in the FRITSCH monomill: the grinding time for the examined samples was 60 s. The average particle size during grinding decreased insignificantly: from 1026 to 344 nm. The corresponding data were obtained by method of dynamic light scattering using a laser analyzer. X-ray diffraction studies showed that the phase composition of the ground powder remained unchanged upon heating in air to 950^{0}C. The difference between $LaMnO_{3+\delta}$ and α-Mn_2O_3 powders produced by mechanoactivation consisted in a pronounced enhancement of the average size of domains with an increase in temperature. In the temperature range from 300 to 700^{0}C the radius varied from 16 to 35 nm (Petrova et al., 2010). We used these data as reference points in analysis of OIE results. At the same time, it was taken into account that sizes of coherent scattering domains during OIE investigations could differ from those established in work (Petrova et al., 2010) owing to different temperatures and duration of heating.

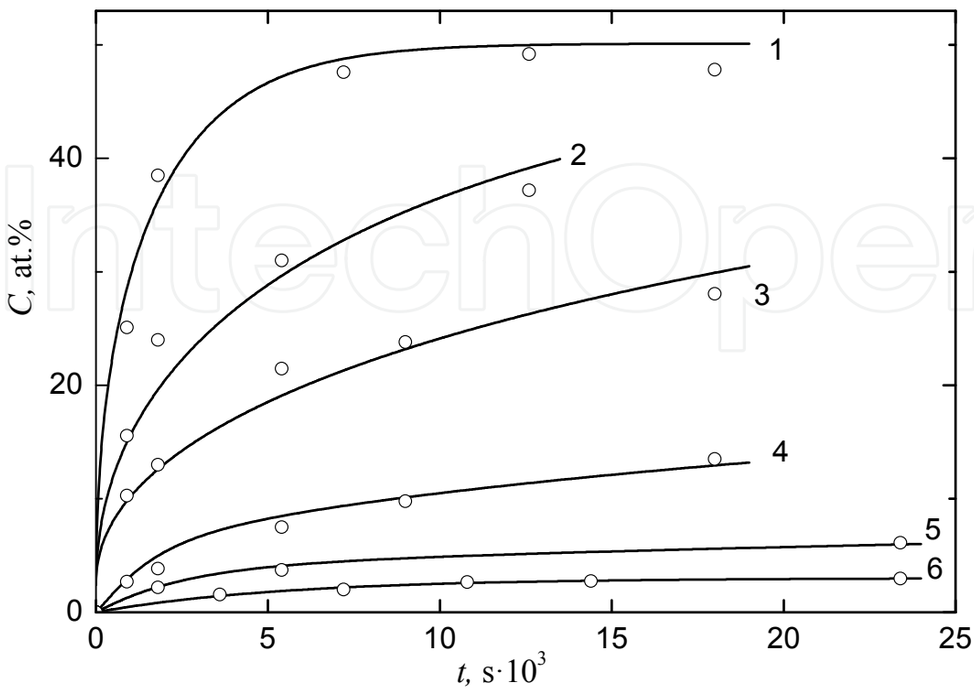

Fig. 4. $C(t)$ dependences for ground powder α-Mn_2O_3: 1, 2, 3, 4, 5, and 6 – results for 700, 550, 500, 400, 350, and 300^{0}C, respectively. Dots – experimental data. Lines – calculation with expression (7) for curves 1, 2, and 3; with expression (4) for curve 6; and in the model for simultaneous relaxation and diffusion for curves 4 and 5. Calculated curve parameters: $D = 0.5 \cdot 10^{-19}$, $0.7 \cdot 10^{-20}$, $1.7 \cdot 10^{-21}$, $1.5 \cdot 10^{-22}$, and $1.5 \cdot 10^{-23}$ m^2/s for 700, 550, 500, 400, and 350^{0}C, respectively; $\Gamma = 0.9 \cdot 10^{-3}$, $5.0 \cdot 10^{-4}$, and $1.8 \cdot 10^{-4}$ for 400, 350, and 300^{0}C, respectively; nanoparticle radii r = 34, 30, 27, 26, 25, and 24 nm for 700, 550, 500, 400, 350, and 300^{0}C, respectively. Δ = 0.5 nm was assumed in the calculations

Experimental and calculated $C(t)$ dependences for the ground powder α-Mn_2O_3 are depicted in Fig. 4. On the whole, the isotope exchange features for $LaMnO_{3+\delta}$ and α-Mn_2O_3 powders prepared by grinding were analogous. This showed up first of all in the fact that the dimensional parameter of the powder responsible for the isotope exchange rate was the X-ray coherent scattering domain radius. However, the OIE parameters for these oxide powders differed drastically. So, at similar temperatures the frequencies Γ (see captions to Figs. 2 and 4) for α-Mn_2O_3 were three to ten times higher than for $LaMnO_{3+\delta}$. Even more dramatic differences were observed for the oxygen volume diffusion coefficients D (see Fig. 5). The data on oxygen diffusion coefficients in manganese oxides were obtained for the first time and can be commented in the following way. The measurement error shown in Fig. 5 was ~50%; it was due mainly to the uncertainty in the powder nanoparticle size in our experiments. We believe that the diffusion coefficient measurement error can be reduced several times if the nanoparticle radius is determined upon each isothermal annealing in gaseous oxygen. Thus, the technique employed can probably provide precision measurements of low values of oxygen volume diffusion in oxides. Of importance is the

following finding. The least typical diffusion length $(Dt)^{1/2}$ in our experiments was about 0.1 nm. This level of measurements can hardly be achieved with other techniques based on concentration profile measurements of light element atoms in solids. Based on the obtained results, we suppose that the use of oxide nanopowders in diffusion experiments will allow one to make a qualitative leap in oxygen diffusion coefficient measurements in oxides.

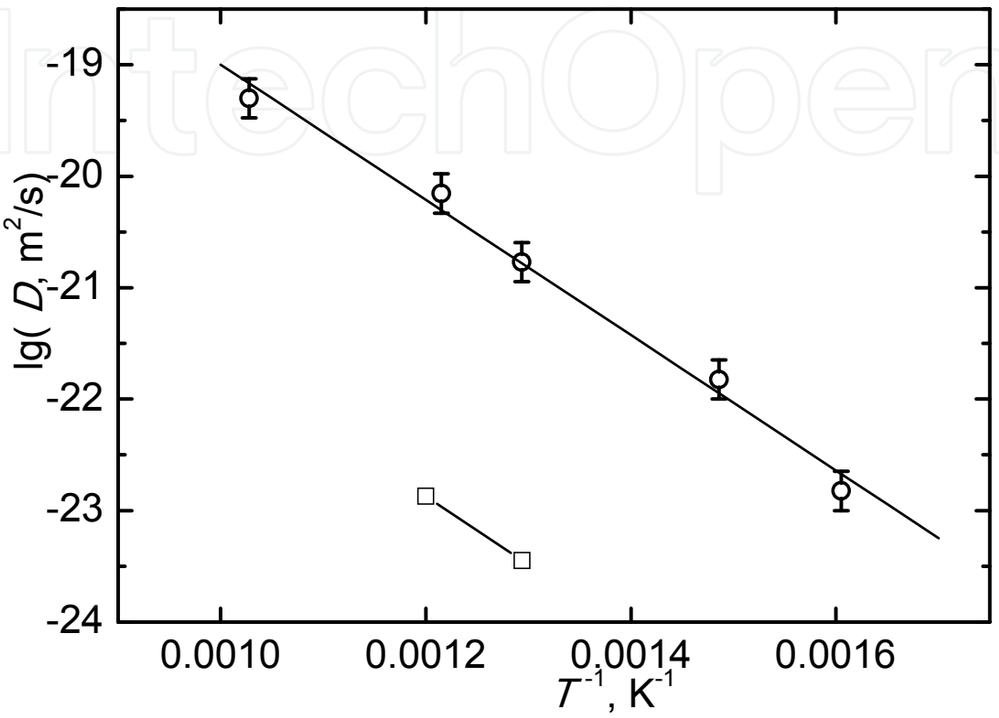

Fig. 5. Temperature dependence of volume diffusion coefficients D in α-Mn_2O_3 (circles) and $LaMnO_{3+\delta}$ (squares)

The oxygen diffusion activation energy in α-Mn_2O_3 was (1.20 ± 0.08) eV. For oxygen diffusion in oxides, this value is typical of oxygen ion migration energy. When oxygen diffusion was due to structural vacancies in the oxygen sublattice of the oxide, approximately the same value was observed also for the volume oxygen diffusion activation energy. For example, in yttrium-stabilized cubic zirconium oxides, oxygen diffusion activation energies were found (Solmon et al., 1995; Brossmann et al., 2004) to be 1.23 and 1.11 eV, respectively. The pre-exponential factor in the temperature versus diffusion coefficient dependence for α-Mn_2O_3 turned out to be very low, namely, $D_0 \approx 10^{-13}$ m²/s. On the basis of this result, the structural oxygen vacancy concentration c_v in the examined manganese oxide can be estimated (Shewmon, 1989) as $c_v \approx D_0/a^2\nu \approx 10^{-6}$ (a – oxide crystal lattice parameter, ν – oxygen ion vibration frequency in the lattice).

In the temperature range 350 – 700^{0}C in α-Mn_2O_3 oxide containing no structural vacancies in the oxygen sublattice, the oxygen diffusion coefficients will be evidently much smaller than those established by the authors, since in oxides without structural vacancies the diffusion activation energy is approximately equal to the sum of migration energy and vacancy formation energy. We don't know any literature data on oxygen vacancy formation energies in manganese oxides.

4.3 Oxygen isotope exchange with cubic zirconium oxide powders

In this section, as distinct from 4.1 and 4.2, we shall consider OIE for gaseous oxygen with an oxide characterized by very fast oxygen volume diffusion coefficients. The condition $(Dt)^{1/2} \gg d$ (d is the particle linear size) corresponding to such species is fulfilled for many oxides containing structural vacancies in the oxygen sublattice.

OIE studies (Fishman et al., 2009) were performed on yttrium-stabilized cubic zirconium oxide YSZ containing 9 mol. % of Y_2O_3. It can be shown that the condition $(Dt)^{1/2} \gg d$ at the minimal isothermal annealing experiment time ($t \approx 10^3$ s) is met not only for nano-, but also for micropowders of this oxide in a wide range of experimental conditions. For example, at 500^0C the oxygen diffusion coefficient value is $5.9 \cdot 10^{-13}$ m^2/c (Solmon et al., 1995) and the typical diffusion length $(Dt)^{1/2}$ is 24 μm. Since at $(Dt)^{1/2} \gg d$ all oxygen ions of the oxide particle take part in isotope exchange, the concentrations of ^{18}O isotopes in the YSZ oxide upon annealing were higher than for $LaMnO_{3+\delta}$. This allowed us to carry out high-accuracy OIE studies on YSZ oxide powders.

YSZ micropowder was produced by coprecipitation of components. For better particle size homogeneity, it was calcined at 1100^0C in air for 3 h. The powder specific surface was 2.15 and 0.64 m^2/g before and after calcination, respectively. Figure 6 displays the experimental and calculated with eq. (9) $C(t)$ dependences for YSZ micropowder. In the calculations we postulated that $\Delta = 0.5$ nm, as in the case of $LaMnO_{3+\delta}$. The experimental and theoretical $C(t)$ dependences are seen to be in reasonable agreement.

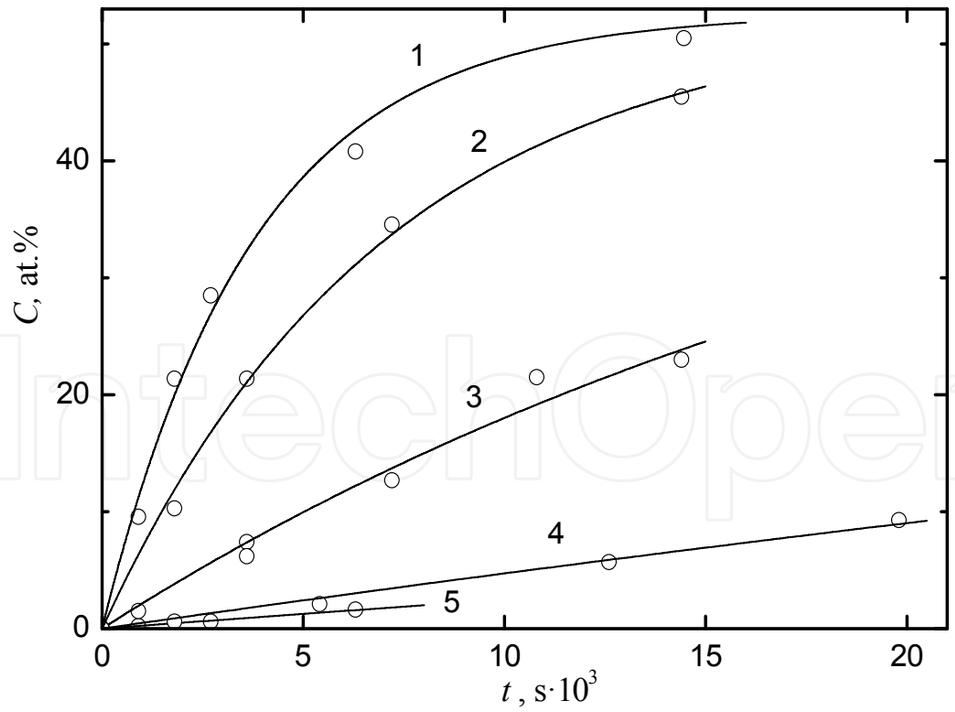

Fig. 6. $C(t)$ dependences for calcined YSZ micropowder. Dots – experiment. Curves – calculation with equation (9). 1, 2, 3, 4, 5 – results at 800, 700, 600, 500, and 450^0C, respectively

The temperature versus frequency Γ dependence is presented in Fig. 7. The frequency factor $\Gamma_0 = 0.84 \cdot 10^3$ s^{-1} and the activation energy E = 0.79 eV correspond to this dependence $\Gamma(T)$. The mean-square error in their determination was 60 and 4%, respectively. These results for the YSZ powder can be compared with the literature data (Manning et al., 1997) obtained in concentration profile measurements for ^{18}O tracer atoms in bulk samples (see eqs. (1)-(2)). These data are also given in Fig. 7 (triangles). In study (Manning et al., 1997), the surface reaction rate was described using the parameter k. Γ was calculated on the basis of k values with eq. (6) at $l = 2 \cdot 10^{-10}$ m. The good agreement of Γ data for the micropowder and the bulk sample of YSZ is indicative of the reliability of the results obtained in works (Fishman et al. 2009; Manning et al., 1997).

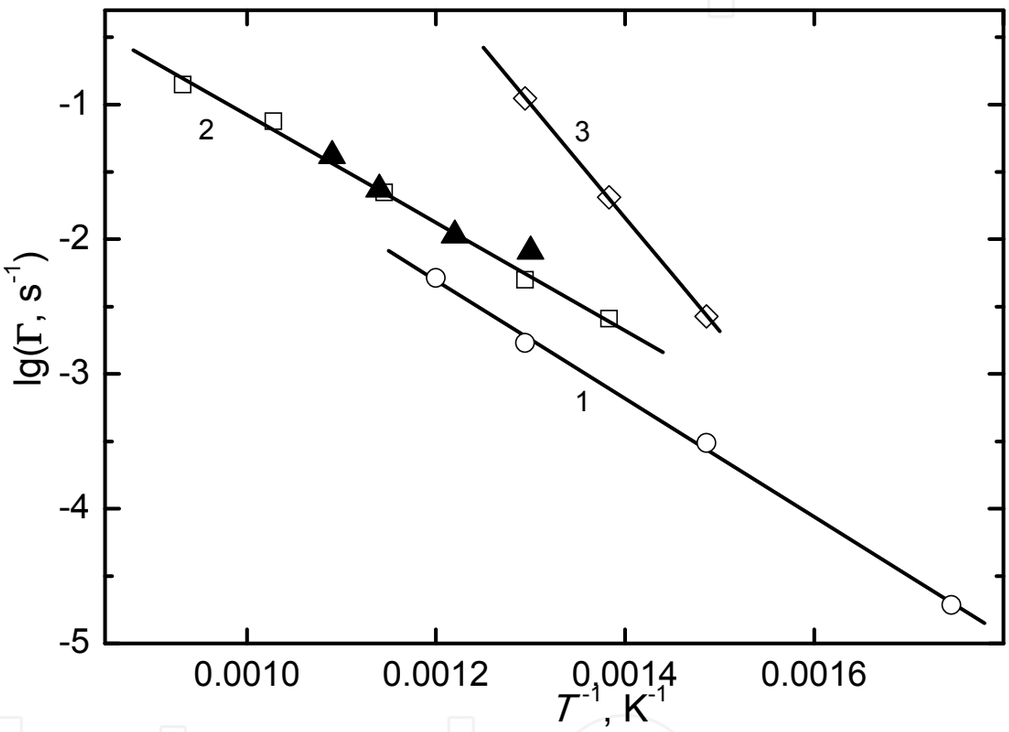

Fig. 7. Temperature dependence of exchange frequency Γ for $LaMnO_{3+\delta}$ nanopowder (line 1), YSZ micropowder (line 2), and nanoboundaries of $LaMnO_{3+\delta}$ (line 3). Triangles – data of work (Manning et al., 1997) for a bulk YSZ sample

Attention is drawn to the very low values of the frequency factor Γ_0 in the temperature versus Γ dependence, which are about 10^3 s^{-1} for $LaMnO_{3+\delta}$ and YSZ oxides. Almost the same frequency factor values were obtained also for bulk samples of other oxides: $La_{0.8}Sr_{0.2}MnO_{3+\delta}$ (De Souza et al., 1999), $La_{0.8}Sr_{0.2}Mn_{1-y}Co_yO_{3\pm\delta}$ (De Souza & Kilner, 1998), $La_{1-x}Sr_xYMnO_{3-\delta}$ (Ruiz-Trejo & Kilner, 1997). These values are by several orders of magnitude smaller than other frequencies characterizing the examined systems. So, the vibration frequency of light atoms in solids is ≥ 10^{12} s^{-1}, whereas the frequency of gaseous molecule collisions with solid particle atoms during isotope exchange is about 10^9 s^{-1}. Such a considerable discrepancy in the characteristic frequency values points to a very low concentration of active centers on the surface of oxides participating in isotope exchange.

Their identification is of current importance. Moreover, such discrepancies in the characteristic frequency values may be due to the existence of several isotope exchange mechanisms, instead of only one mechanism of dissociation adsorption – desorption (Odzaki, 1979).

The YSZ nanopowder containing 9.5 mol. % Y_2O_3 was produced by laser sputtering of a ceramic target (Ivanov et al., 2006). It was subjected to sedimentation in isopropyl alcohol to remove particles with diameter of 200 nm or larger from the powder. The specific surface of the nanopowder was (58.6 ± 0.4) m^2/g. Upon annealings at 500^0C, it decreased to (53.3 ± 0.8) m^2/g, which is likely to be connected with agglomeration of smaller particles.

The experimental and calculated $C(t)$ dependences for the YSZ nanopowder are exhibited in Fig. 8 (Fishman et al., 2009). Comparing the experimental data in Figs. 6 and 8 we see that the nanopowder is characterized by higher ^{18}O isotope concentrations, which were also observed for other oxides. The calculated curve 2 in Fig. 8 was plotted with expression (11). In the calculations we used powder particle size distribution established by transmission electron microscopy (Ivanov et al., 2006); it was narrow with the width of about 13 nm and had a maximum at the particle diameter of 11 nm. It was also assumed that the isotope exchange frequencies Γ are not different for nano- and micropowders. From Fig. 8 it is seen that the calculated (curve 2) and experimental $C(t)$ dependences do not agree with each other. At the same time, the powder specific surface calculated with the above nanopowder particle size distribution (58.1 m^2/g) practically coincided with its experimental value (58.6 m^2/g). The agreement between theoretical and experimental $C(t)$ results was not improved when possible changes in the frequency Γ in going from micro- to nanopowder were taken into account. The experimental $C(t)$ dependence was not at all described by theoretical expressions supposing a narrow powder particle size distribution.

It was suggested on the basis of these results that the discrepancy in the calculated and experimental $C(t)$ data is due to the existence of large particles in the nanopowder, which were not presented in the size distribution function of powder particles obtained with transmission electron microscopy. The corresponding calculation had an evaluating character, where all large particles were postulated to have a spherical shape and similar size. The calculations showed that a satisfactory fit between calculated and experimental $C(t)$ dependences can be achieved within this model. Figure 8 (curve 1) demonstrates one of the model versions postulating the presence of particles with radius 130 nm in the nanopowder. Their part in the total number of particles was estimated to be 0.0003. A similar satisfactory agreement between calculated and experimental $C(t)$ data was achieved for large particle radii ranging from 100 to 130 nm. However, this interpretation of the experimental $C(t)$ data was in conflict with the specific surface experimental data. It was calculated that the nanopowder containing particles with a 130 nm radius would have the specific surface 20.4 m^2/g if the part of large particles is 0.0003 (the experimental value being 53.3 m^2/g).

The problems of interpretation of experimental data on specific surface for nanopowders produced by laser sputtering of a ceramic target were also known earlier. They manifested themselves in the following result: the specific surface of sedimentated and non-sedimentated powders were virtually the same according to numerous studies. For example, in work (Kotov et. al., 2004) the specific surface of sedimentated and non-sedimentated $Ce_{0.78}Gd_{0.22}O_{2-\delta}$ nanopowder was found to be 57 and 56 m^2/g, respectively, though the non-sedimentated powder contained to 8 mass % of large particles. Such results

are usually explained in the following way: during sedimentation both large and finest particles are removed. However, this explanation seems doubtful. Some estimations show that small differences in the specific surface for sedimentated and non-sedimentated powders can occur only in the case of multi-layer coating of large particles with nanoparticles. According to the available data, less than one nanoparticle layer on large particles was usually registed on photographs.

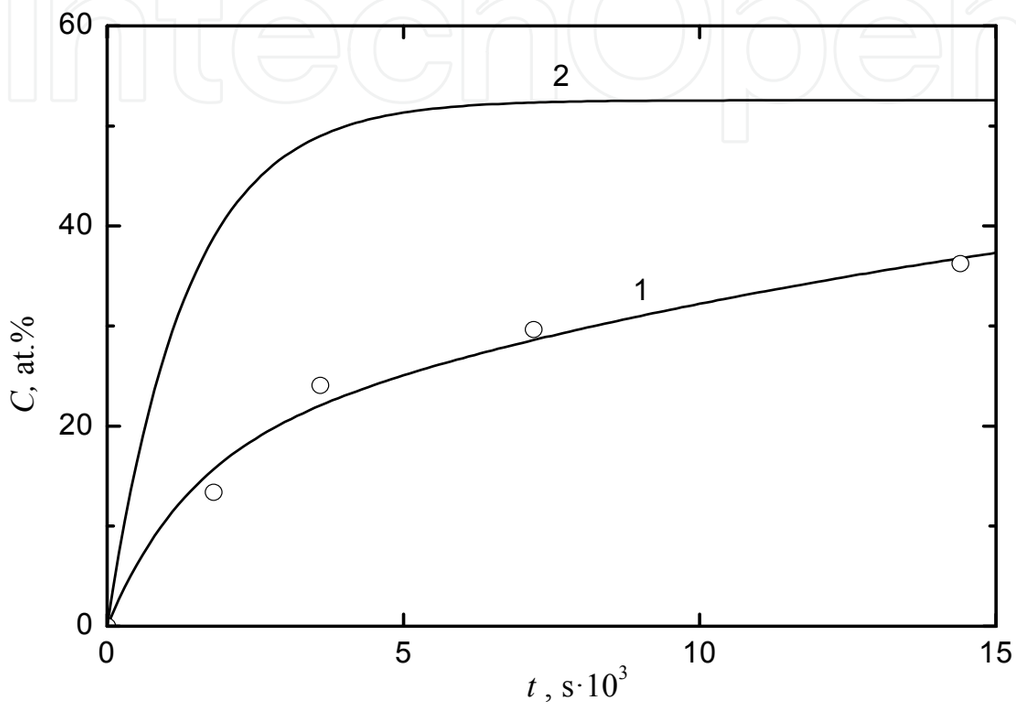

Fig. 8. $C(t)$ dependences for the YSZ nanopowder at 500^{0}C. Dots – experiment; curves 1 and 2 – calculation with equation (11). Curve 2 – calculation with the particle size distribution function obtained by transmission electron microscopy. Curve 1 – calculation with the particle size distribution function obtained by transmission electron microscopy and supplemented by the presence of particles with the radius of 130 nm

It can be supposed as an alternative that large YSZ particles appearing during laser sputtering of a ceramic target are conglomerates of usual nanoparticles. When the BET technique is used, nitrogen molecules penetrate into the space between nanoparticles contained in large particles. That is why the specific surface values for non-sedimentated and sedimentated nanoparticles are almost the same. At the same time, the presence of large particles in nanopowder was reliably established with the OIE technique. These findings show that the OIE technique can yield supplementary (as compared with the BET method) information about the dimensional characteristics of powders and is very sensitive to the presence of small amounts of large particles in nanopowder, which lie beyond the main peak of the size distribution function of powder particles. According to these results, the expected sensitivity of the isotope exchange technique is about 0.01% of the number of particles.

4.4 Oxygen isotope exchange with aluminum oxide nanopowders

In this section we consider OIE in nanopowders produced by electrical explosion of wire. The powders were sedimentated in isopropyl alcohol. The sedimentation regime provided removal of particles with diameter greater than 200 nm from the powder. The main characteristics of the powders are listed in the Table 1.

S, m^2/g	d_{BET}, nm	γ-Al_2O_3/δ-Al_2O_3	d_x, nm	d_p, nm	Θ, nm
23.2	73	30/70	18.5	16	19
38.3	45	40/60	17	17	24
41.7	40	15/85	21	-	-
84	20.5	53/47	21	13	13

Table 1. Characteristics of aluminum oxide powders

The values of specific surface S were determined with the BET method; the nanoparticle diameter d_{BET} was calculated with the expression $d_{BET} = 6/S\rho$, where ρ is the calculated density for the crystalline component of the powder. X-ray phase analysis data showed that all the powders contained two crystalline phases: γ-Al_2O_3 and δ-Al_2O_3. The ratios of their mass fractions are presented in the Table 1. X-ray powder diffraction patterns were also indicative of an amorphous component; however, its amount in the powders could not be determined. The tabulated sizes d_x of X-ray coherent scattering domains characterize the δ-Al_2O_3 phase. The size distribution functions of powder particle were determined using transmission electron microscopy. All the distributions featured a narrow peak; its widths Θ and the most probable particle diameters d_p are also listed in the Table 1.

As is seen from the Table 1, the aluminum oxide nanopowders are much more complicated objects than those examined in sections 4.1, 4.2, and 4.3. Since the OIE technique for nanopowders made a good showing in the case of relatively simple oxide systems (see the above sections), it is interesting to apply this method to more complicated species. The major task in this section was to estimate the sensitivity of the OIE technique to the multi-phase state of nanopowders and, in particular, to the presence of an amorphous phase.

$C(t)$ dependences at 500^0C for OIE of aluminum oxide nanopowders with $^{18}O_2$ are depicted in Fig. 9. For one of the oxides (with specific surface of 41.7 m^2/g), investigations were also performed for a powder, which was not exposed to preliminary stabilization annealing in air. In this case, the concentrations $C(t)$ were appreciably higher than for the stabilized powder. This finding points to a nonstoichiometric chemical composition of the aluminum oxide powders produced by electric explosion of wire. Such peculiarities of nanooxides can be easily revealed with the NRA method.

The $C(t)$ dependences in Fig. 9 differ from those for other nanopowders in appreciably lower ^{18}O concentrations. This hampered experimental studies of IOE kinetics at temperatures, for which the nanoparticle agglomeration effect can be disregard. For this reason, the main body of OIE data for aluminum oxides was obtained with the use of carbon dioxide CO_2 enriched with ^{18}O isotopes, rather than with gaseous oxygen. As was shown in section 4.1, replacement of $^{18}O_2$ by $C^{18}O_2$ led to an increase in the ^{18}O isotope concentration in $LaMnO_{3+\delta}$ powders. The same effect is also observed for aluminum oxide nanopowders, which

permitted us to perform $C(t)$ dependence measurements in the temperature range from 500 to 100^{0}C. Figure 10 shows $C(t)$ dependences for the powder with specific surface 38.3 m^2/g. For other powders, $C(t)$ dependences were analogous, namely, the concentration of ^{18}O isotopes in the powders increased with the time and temperature of annealing and powder specific surface.

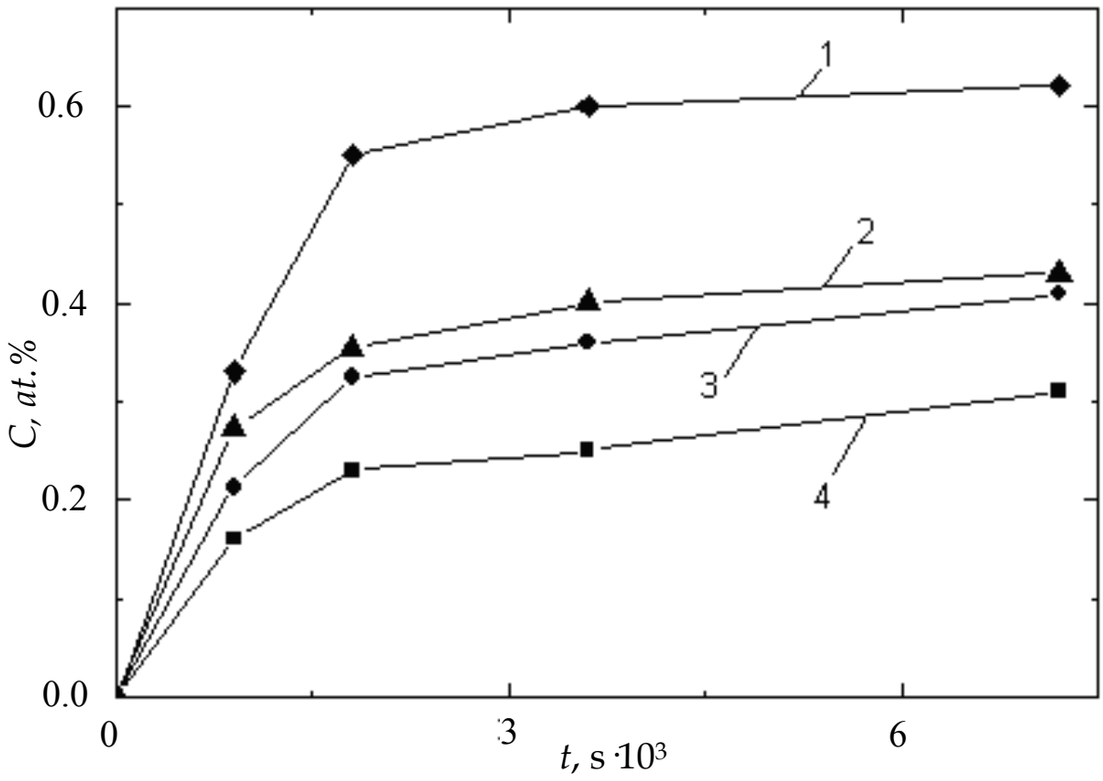

Fig. 9. Experimental $C(t)$ dependences for aluminum oxide nanopowders at 500^{0}C. 1,3,4 – results for powders with specific surface 84, 41.7, and 23.2 m^2/g, respectively. 2 – results for the powder, which was not exposed to preliminary stabilization annealing in air, its specific surface is 41.7 m^2/g

Figure 11 demonstrates several $C(S)$ dependences of ^{18}O isotope concentration versus the powder specific surface S. For each dependence, the time and temperature of annealing in the atmosphere of tracer atoms were constant. All the $C(S)$ dependences, including those not given in Fig. 11, were linear. As is seen in Fig. 11, for the systems powder - $^{18}O_2$ they are fulfilled to a very high accuracy, while for the systems powder - $C^{18}O_2$ a more considerable deviation form the linear dependences is observed. Thus, it can be stated quite definitely that for multiphase oxide powders the concentration of ^{18}O isotopes during isotope exchange is also a linear function of the powder specific surface. Note that at 500^{0}C the extrapolation of $C(S)$ dependences to the region $S\rightarrow 0$ gives values $C(S\rightarrow 0) \neq 0$. This is likely to be due to oxygen diffusion in nanopowders. This peculiarity of $C(S)$ dependences can be used for the estimation of oxygen diffusion coefficients in aluminum oxides at 500^{0}C.

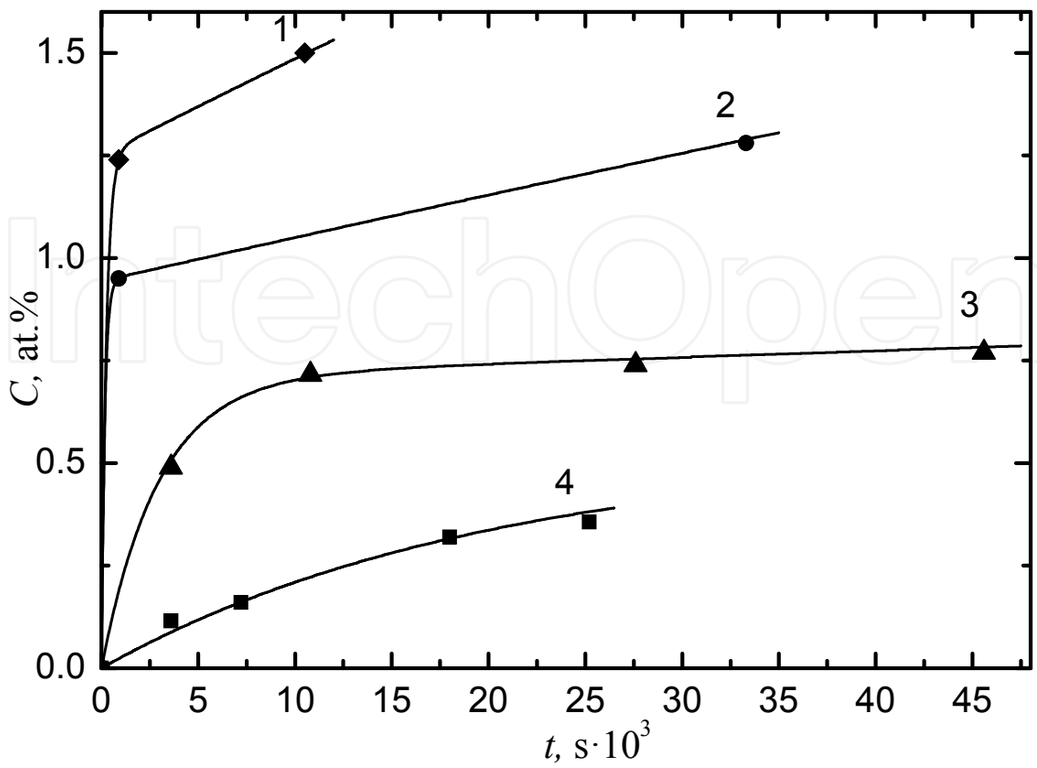

Fig. 10. $C(t)$ dependences for aluminum oxide nanopowder during annealing in carbon dioxide enriched with ^{18}O isotopes. Dots – experimental data. 1,2,3,4 – results for 500, 400, 200, and 100^{0}C, respectively. Curves – calculation with equation (14). Calculated curve parameters: Δ_2 = 0.66 nm, α_1 = 0.13, Γ_1 = 5.0 ·10^{-5}, 3.4 ·10^{-4}, 6.0 ·10^{-3}, and 1.0 ·10^{-2} s^{-1}, Γ_2 = 2.5 ·10^{-8}, 3 ·10^{-7}, 2.6 ·10^{-6}, and 0.57 ·10^{-5} s^{-1}, Δ_1 = 0.66, 0.88, 1.17, and 1.55 nm at 100, 200, 400, and 500^{0}C, respectively

Thus, some OIE regularities for single- and multi-phase oxide nanopowders were found to be of the same type. This is true for linear $C(S)$ dependences and the effect of the oxygen-containing gas type on ^{18}O isotope concentrations. At the same time, multi-phase aluminum oxide powders exhibited some features that distinguished them from other examined systems, namely, the aforementioned low level of ^{18}O isotope concentrations in powders upon annealing in $^{18}O_2$. When the gaseous atmosphere was changed to $C^{18}O_2$, the concentrations of ^{18}O isotopes increased, but still remained low as compared with those for oxide powders earlier considered. Moreover, the $C(t)$ concentrations for aluminum oxides powders were also unusual (see Fig. 10). They were described neither by relaxation-type expressions (4)-(5), nor by the model for simultaneous relaxation and diffusion. The same is true of the attempts to explain the experimental $C(t)$ data by the presence of larger particles in aluminum oxide powders, which are not present in the main peak of size distribution function of powder particles.

No strict theoretical description of $C(t)$ data could be given for aluminum oxides since IOE in amorphous oxide phases has not been studied at all. Therefore let us analyze $C(t)$ dependences in a crude model, which allows for the multi-phase character of aluminum oxide powders and, especially, for the presence of an amorphous phase in them. For this

phase we postulate that the number of oxygen ions participating in isotope exchange between the amorphous phase and the gaseous atmosphere increases with temperature. It means that parameter Δ in eqs. (4)-(5) for the amorphous phase increases with temperature too. We shall also restrict our analysis to the model considering only two – amorphous and crystalline – phases. True, X-ray structural analysis revealed the existence of two crystalline phases: γ-Al_2O_3 and δ-Al_2O_3. However, the approximation proposed for aluminum oxide powders may be acceptable since no noticeable distinctions were observed in the $C(t)$ dependences for powders with close specific surface values (38.3 and 41.7 m^2/g) and with drastically different volumes of γ-Al_2O_3 and δ-Al_2O_3 phases (see the Table 1). Assume that the oxygen diffusion rate in oxide particles is negligibly small (at least for $T < 500^0$C).

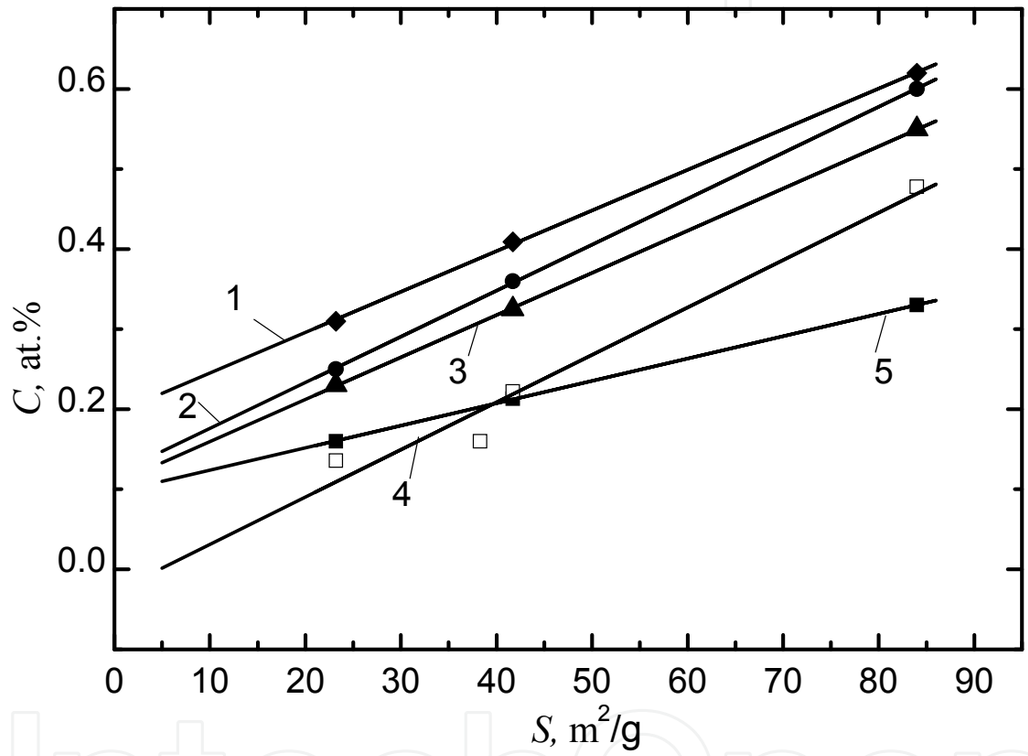

Fig. 11. Average ^{18}O isotope concentration C in aluminum oxide nanopowders as a function of the powders specific surface S during annealing in oxygen and carbon dioxide enriched with ^{18}O isotopes. Annealing conditions: 1,2,3,4 – annealing in $^{18}O_2$ at 500^0C for 120, 60, 30 and 15 min., respectively; 5 – annealing in $C^{18}O_2$ at 100^0C for 120 min

In terms of the above approximations, the expression for $C(t)$ is a sum of relaxation-type contributions (see eq. (5)) from amorphous and crystalline powder components

$$C(t) = C_0 S\left[\alpha_1\rho_1\Delta_1\left(1-\exp(-\Gamma_1 t)\right) + \alpha_2\rho_2\Delta_2\left(1-\exp(-\Gamma_2 t)\right)\right] \quad , \tag{12}$$

where indexes 1 and 2 relate to the oxide powder amorphous and crystalline phases, respectively; $\alpha_{1,2}$ – parts of these phases in the total surface area of the powder ($\alpha_1 + \alpha_2 = 1$). The results of $C(t)$ calculations with eq. (14) are given as solid lines in Fig. 10. The values of parameters α_1, Δ_1, Δ_2, Γ_1, and Γ_2 are presented in the caption. In the calculations we also took

into consideration that the densities of the aluminum oxide amorphous phase, the γ-Al_2O_3 phase and the δ-Al_2O_3 phase are 3.0, 3.35 and 3.62 g/cm^3, respectively.

It is seen that the "two-phase" model easily provides a satisfactory description of experimental $C(t)$ dependences during isotope exchange for a powder with specific surface 38.3 m^2/g at all temperatures. Such a satisfactory description should be obtained also for powders with other specific surface values (all model parameters being the same) owing to the linear dependence $C(S)$. No special problems are expected also in the description of $C(t)$ dependences for isotope exchange in aluminum oxides - $^{18}O_2$ systems by means of eq. (12). However, the hypothesis that the number of oxygen ions in the amorphous phase surface layer participating in isotope exchange depends on the annealing temperature requires special experimental verification.

Thus, the studies of aluminum oxide powders with complex phase compositions showed that the OIE technique is very sensitive not only to the particle size of nanopowders, but probably to the presence of an amorphous phase in them.

5. Oxygen grain boundary diffusion and oxygen isotope exchange in nanocrystalline oxide $LaMnO_{3+\delta}$

Grain boundary diffusion in metal oxides is a poorly studied phenomenon and the data from different authors are controversial. In some of the most reliable works, the presence of enhanced diffusion at the grain boundaries is questioned (Kaur et al., 1995). At the same time, this fact has been reliably determined for metallic systems. The question of the possible common properties of the grain boundary diffusion for oxides and metals is still open. New experimental data on the coefficients of grain boundary diffusion in oxides attract the interest of theoreticians due to the specific properties of the grain boundaries in ionic compounds; in particular, these boundaries are charged. The investigations under consideration are of an applied interest, because metal oxides are widely used as functional materials in applications. The coefficients of the grain boundary diffusion determine the stability of the properties of polycrystalline materials. Presently, most researchers explain this inadequate situation with the diffusion data for oxides citing methodological reasons. It is difficult to obtain correct results primarily because of the strong influence of impurities in the oxides (Kaur et al., 1995). Control of the purity and stoichiometry of a material, especially near grain boundaries, is a complicated problem. In this connection, the study (Vykhodets et al., 2008) dealt with the problem of obtaining correct data on grain boundary diffusion in oxides.

The measurements were carried out for $LaMnO_{3+\delta}$ oxide. This is a suitable model object, because it does not have structural vacancies in the oxygen sublattice. Similar systems are characterized by low values of the volume diffusion coefficients of oxygen D. This facilitates the choice of the annealing regimes for which the contribution of the grain boundary diffusion to the formation of the concentration profiles for the tracer atoms will be determinative. The research was focused on the realization of two kinetic regimes: the B type, when the grain boundary diffusion and volume diffusion take place simultaneously; and the C type, when the diffusion of the tracer atoms into the bulk of grains is negligible. Such an approach allows one to determine two parameters characterizing grain boundary diffusion: the diffusion coefficient for grain boundaries D_{GB} and the boundary width δ (Kaur et al., 1995).

The research was carried out for nanocrystalline samples. For them, the conditions to obtain reliable results are more favorable due to the presence of the branching net of the boundaries, which enhances the contribution of the grain boundary diffusion to the diffusion flux. Besides, the nanocrystalline samples were prepared with the method in which the time of the nanostructure formation is very short. This requirement is fulfilled by the shockwave loading method (Kozlov et al., 1997) using explosives. In this case, it is expected that the doping of the nanograin boundaries is weak or absent. The initial material for the shockwave method is a coarse-grained powder of $LaMnO_{3+\delta}$ with 15–30-μm grains. According to the results of x-ray diffraction analysis, the material obtained after an explosion was nanocrystalline with an average particle size of 41 nm. These characteristics did not change after further diffraction annealing. Samples 3-mm-thick with an area of 1 cm^2 were cut out of this material. Mechanical operations of cutting, polishing, etc., were not performed to avoid the surface contamination of the samples. The scanning electron microscopy investigation of the fractured surface of the samples revealed that the main element of the microstructure of the samples under consideration is a crystallite with an average size of 3μm. The distance between the crystallites was very large (submicron); as a result, $^{18}O_2$ molecules penetrate freely into the space between the crystallites during annealing. This feature was taken into account in mathematical treatment of $C(x)$ profiles.

The results presented in Fig. 2 allow one to choose the optimal conditions for the diffusion annealing of compact samples. At 500^0C, the C and B kinetic types are expected for $t \le 1$ h and for a few hours, respectively. The concentration of ^{18}O atoms near the surface of the samples should be less than $(3/2)C_0\Delta/r$ in the C regime and about or larger than this value in the B regime. This estimate was obtained by taking into account that, in contrast to an insulated nanoparticle, one boundary inside the massive sample simultaneously belongs to two particles. Similarly, the optimal conditions of annealing were also determined for other temperatures. Diffusion annealings were performed at 500, 450, and 400^0C for ~ 1, 4, and 26 h, respectively, to realize the C type kinetics. At 500^0C, diffusion annealings for ~4 and 8 h oriented to the B type kinetics were carried out.

The concentration profiles $C(x,t)$ of ^{18}O atoms for bulk samples (some of them are shown in Fig. 12) were determined with the NRA method, the measurement conditions being the same as for powders (see section 4.1). The concentration profiles were characterized by the presence of background concentration $C_{PH}(t)$. It appears due to the free penetration of ^{18}O molecules into the space between crystallites during annealing. It is easy to show that the following relation should be fulfilled in this case: $N(t)/C_{PH}(t) = n/4$, where $N(t) = \int_0^\infty dx\left(C(x,t) - C_{PH}(t)\right)$, n is the linear size of a crystallite. The experimental value of $N(t)/C_{PH}(t)$ for ~1-, 4-, and 8-h annealing did not differ within the statistical error (~6%) and the average value of the parameter n was approximately 3 μm. This value is in agreement with the results of the investigations of the microstructure of the samples. Thus, there is good reason to believe that the difference profiles ($C(x,t)$ - C_{PH}) were due to diffusion into crystallites of size ~3 μm, which, in their turn, have a nanocrystalline structure.

In $C(x,t)$ profiles processing, expression (1) was used for the C regime. Here, the volume diffusion coefficient D was replaced by the grain boundary diffusion coefficient D_{GB} and it

was assumed that $C_S^{max} = 3C_0\Delta/2r = 1.75$ at. %. For the B regime, the following expression (Kaur et al., 1995) was used for $C(x,t)$ profiles processing:

$$D_{GB}\delta = 1.332(D/t)^{1/2}(\partial \ln C(x)/\partial x)^{-2} \quad , \tag{13}$$

where δ is the grain boundary width. Expression (13) satisfactorily describes the corresponding experimental data within measurement error.

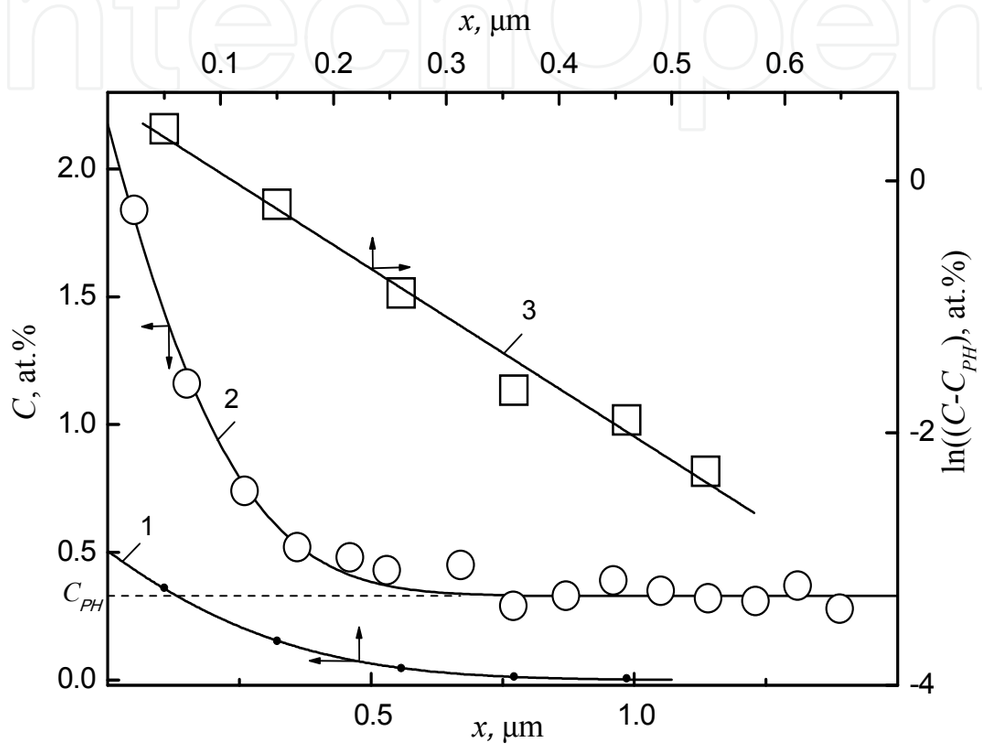

Fig. 12. Concentration profiles of ^{18}O atoms in $LaMnO_{3+\delta}$ nanocrystal: 1 - 400^{0}C, t = 26 h, curve – calculation by eq. (3), background C_{PH} is deducted; 2 - 500^{0}C, t = 4 h 11 min., curve – experimental dependence; 3 - 500^{0}C, t = 8 h 12 min.; dots – experiment

Figure 13 shows the results of temperature versus grain boundary diffusion coefficients studies. The grain boundary diffusion activation energy Q_{GB} was found to be 1.95 eV. Using the data of study (De Souza et al., 2000) for volume diffusion activation energy Q_V we find $Q_{GB} \approx 0.7Q_V$. Such a relationship is typical of metallic systems for vacancy-type diffusion (Kaur et al., 1995). Thus, no qualitative differences in the diffusion behavior for oxide and metallic systems were established.

A value of 0.044 nm was found for boundary width δ. It is an order of magnitude larger than the value δ ≈ 0.5 nm obtained in all of the correct experiments on grain boundary diffusion. Note that using eq. (13) one can only determine an effective thickness of the boundary, δ, disregarding its structure and, correspondingly, diffusion inhomogeneity. For an inhomogeneous boundary with the mixing of tracer atoms between intervals with strong disordering (dislocation cores) and with a weakly distorted lattice, the ln $C(x)$ dependence is

linear (Kondrat'ev & Trakhtenberg, 1986), as in the case of the homogeneous boundary. The left-hand side of Eq. (13) is reduced to the form $D_{GB}\delta p$, where p is the volume fraction of the trajectories with a high diffusion permeability. It is seen that the δ value for $p \ll 1$ is strongly underestimated. We can point out some reasons why the structural inhomogeneity of the boundaries was manifested in our experiments. This can be associated with a specific type of nanoboundaries formed in a brittle material after shock loading and with a short diffusion length $(Dt)^{1/2}$, which was on the order of the atomic size in our experiments.

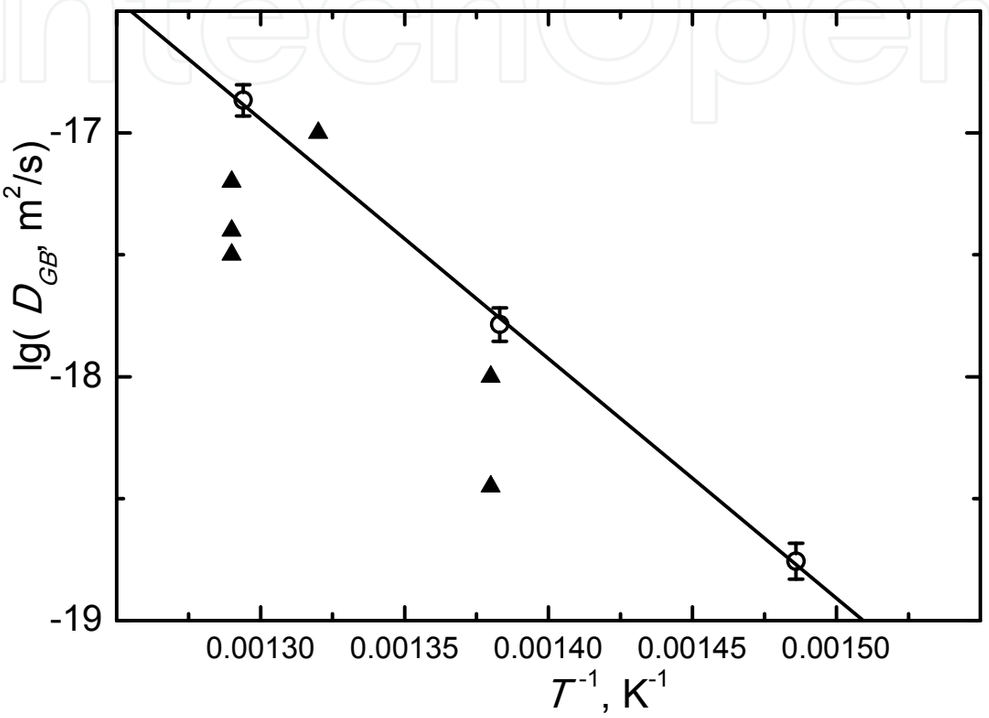

Fig. 13. Temperature dependence of grain boundary diffusion coefficients D_{GB} in $LaMnO_{3+\delta}$ nanocrystal. Triangles – results of work (Brossmann et al., 2004) for ZrO_2 nanocrystal

We know only one work (Brossmann et al., 2004) devoted to oxygen grain boundary diffusion in oxide nanocrystalline. This study was performed on a high-purity oxide ZrO_2. The ZrO_2 nanocrystalline was produced by sintering of oxide nanoparticles with the average nanograin size 100 nm. Diffusion was examined with the use of the B type kinetics; the grain boundary width value δ = 0.5 nm was postulated for determination of grain boundary diffusion coefficients D_{GB}. The value of Q_{GB} = 1.95 eV obtained in work (Brossmann et al., 2004) coincided with the result of study (Vykhodets et al., 2008). In both works, enhanced grain boundary diffusion was registered. The D_{GB} values from work (Brossmann et al., 2004) are given in Fig. 13 for comparison. The oxygen grain boundary diffusion coefficient in ZrO_2 and $LaMnO_{3+\delta}$ nanocrystallines are seen to be very similar. This coincidence of the results reported in the two works (Brossmann et al., 2004; Vykhodets et al., 2008) is considered to be accidental; nevertheless, we draw attention to these facts. Thus, an important finding for the diffusion theory has been obtained in the above studies, namely, no qualitative differences in volume and grain boundary diffusion were found for oxide and metal systems. Note that both studies were performed on nanocrystallines; besides, systematic measurement errors

due to uncontrolled doping of oxide grain boundaries with impurities were probably excluded.

As was mentioned above, the grain boundary diffusion coefficients D_{GB} in study (Vykhodets et al., 2008) at 500, 450, and 400^0C were determined with the use of the C type kinetics, i.e. in the absence of oxygen volume diffusion. By means of expressions (1), (2), and (6) we calculated for the same temperature the parameters *H, k*, and Γ characterizing the surface energy barrier during isotope exchange of gaseous oxygen with $LaMnO_{3+\delta}$ oxide nanoboundaries (Fishman et al., 2010). The results for Γ are given in Fig. 7. As in section 4.3, the *k* values were recalculated in Γ using expression (6) at $l = 2 \cdot 10^{-10}$ m. Figure 7 shows a great difference in the frequency factor Γ_0 and activation energy *E* values in the temperature versus Γ dependence, which were obtained, respectively, for the nanograin boundary and the regular lattice of $LaMnO_{3+\delta}$. The difference is almost 7 orders of magnitude for Γ_0 ($0.9 \cdot 10^{10}$ and $0.97 \cdot 10^3$ s^{-1}) and 2 times for *E* (1.67 and 0.88 eV). In our opinion, such a dramatic difference in Γ_0 and *E* parameters for the nanograin boundary and the regular lattice of one and the same oxide is difficult to understand from the isotope exchange mechanism only. Competing mechanisms can take place simultaneously, and, depending on the relationship between the system parameters, one or another mechanism will prevail. A similar situation happens, for example, in studies of diffusion in solids, when volume and grain boundary diffusion occur simultaneously. For such objects, the contributions from volume and grain boundary diffusion to the mass transfer rate will depend on the experiment conditions; as a result, drastically different values of effective diffusion coefficients, activation energies, and frequency factors in the temperature dependence *D* can be obtained.

6. Conclusion

In the studies presented here it was shown that the OIE parameters are sensitive to the dimensional characteristics of oxide powders. Therefore, the approach based on OIE examination shows promise for receiving the information about the size of nanopowder particles. Similar data are obtained with other techniques (electron microscopy, X-ray diffraction, specific surface measurement, dynamic light scattering by means of a laser analyzer etc.); in this respect, the OIE technique has an important specific feature. In addition to the conventional methods, it makes it possible to determine the stoichiometry of oxide powders, is sensitive to chemical activity of powders and, probably, to the presence of amorphous phases and very small amounts of larger particles in nanopowders. These peculiarities of the considered technique are of great interest both for theory and practice, since all existing technologies for nanopowder synthesis lead to the formation of non-equilibrium materials and assemblies consisting of particles with different sizes and shapes. Moreover, when the OIE technique is used on nanopowders, very low oxygen volume diffusion coefficient values can be measured as compared with traditional approaches. The application of the OIE technique for bulk nanocrystalline samples also holds much promise. Already in several works it was shown that considerable progress can be achieved with the use of this technique in the examination of oxygen grain boundary diffusion in oxides.

7. Acknowledgment

This work was supported by RFBR (grant 10-03-96016-p_ural_a and grant 09-03-00335_a), the Program of fundamental research of Presidium of Russian Academy of Sciences N 27

"Foundations of fundamental research of nanotechnology and nanomaterials" and the Federal Target Program "Scientific and scientific-pedagogical staff of innovation Russia (contract 02,740. 11.0641).

8. References

Brossmann, U. et al. (2004), Oxygen diffusion in nanocrystalline ZrO_2, Rev. Adv. Mater. Sci., Vol. 6, p. 7-11, ISSN 1605-8127

Carter, S. et al. (1992), Oxygen transport in selected nonstoichiometric perovskite structure oxides, Solid State Ionics, Vol. 53-56, p. 597-605, ISSN 0167-2738

De Souza, R.A. & Kilner, J.A. (1998), Oxygen transport in La_{1-x} $Sr_xMn_{1-y}Co_yO_{3\pm\delta}$ perovskites - Part I. Oxygen tracer diffusion, Solid State Ionics, Vol. 106, p.175-187, ISSN 0167-2738

De Souza, R.A. et al. (2000), A SIMS study of oxygen tracer diffusion and surface exchange in $La_{0.8}Sr_{0.2}MnO_{3+\delta}$, Materials Letters, Vol. 43, p. 43-52, ISSN 0167-577X

Fishman, A.Ya. et al. (2003), Diffusion in concentrated Jahn-Teller systems, Advances in quantum chemistry, Vol. 44, p.497- 509, ISBN: 0-12-034844-6, ISSN 0065-3276

Fishman, A.Ya. et al. (2009), Oxygen isotope exchange in nanocrystal oxides Journal of NanoResearch, Vol.7, p. 33-41, ISSN 1662-5250

Fishman, A.Ya. et al. (2010), Isotope Exchange between Gaseous Oxygen and Nano-Grain Boundary of $LaMnO_{3+\delta}$ Oxide, Defect and Diffusion Forum, Vol. 297-301,p. 1301-1305, ISSN 1012-0386.

Gizhevskii, B.A. et al, (2008), Oxygen Isotope Exchange Between the Gaseous Phase Enriched with the ^{18}O Isotope and Nanocrystal Oxides $LaMnO_{3+\delta}$ Obtained By Severe Plastic Deformations, Defect and Diffusion Forum, Vol.273-276, p.233-238, ISSN 1012-0386

Ivanov, M.A. et al. (2006), Formation of a thin-layer electrolyte for SOFC by magnetic pulse compaction of tapes cast of nanopowders, Journal of Power Sources, Vol. 159, p. 605-612, ISSN 0378-7753

Kaur, Y et al. (1995), *Fundamentals of Grain and Interphase Boundary Diffusion* (3rd ed.) Wiley, ISBN 978-0-471-93819-4, New York, USA

Kondrat'ev, V.V. & Trakhtenberg, I. Sh. (1986), Grain-boundary diffusion of atoms in a model of structurally heterogeneous boundary, The Phys. Metal & Metallogr., Vol. 2, p. 434-441, ISSN 0031-918X

Kotov, Yu.A. et. al. (2004), Characteristics of nanopowders produced by vaporation CeO_2/Gd_2O_3 emission targets repetitively pulsed CO_2 laser, Journal of Technical Physics, Vol. 74, N3, p.72-77, ISSN 0044-4510

Kozlov, E. A. et al. (1997), Patent of Russian Federation No. 2124716, December 24, 1997

Manning, P.S. et al. (1997), The kinetics of oxygen transport in 9.5 mol % single crystal yttria stabilized zirconia, Solid State Ionics, Vol. 100, p. 1-10, ISSN 0167-2738

Odzaki, A. (1978), *Isotopic studies of heterogeneous catalysis,* Acad.Press, ISBN 0125319509, New York, USA

Routbort, J.L. et al. (1997), Diffusion-controlled creep in mixed-conducting oxides, Def. and Dif. Forum, Vol. 143-147, p.1201-1205, ISSN 1012-0386

Ruiz-Trejo, E. & Kilner, J.A. (1997), Oxygen diffusion and proton conduction in $La_{1-x}Sr_xYO_{3-\delta}$, Solid State Ionics, Vol. 97, N 1-4. - P. 529-534, ISSN 0167-2738

Petrova, S.A. et al. (2010), Phase states of mechanoactivated manganese oxides, *Proceedings of the Ninthight Israeli - Russia Bi-National Workshop 2010 "The optimization of composition, structure and properties of metals, oxides, composites, nano and amorphous materials*", p. 138-152, Belokurikha, Russia, July 25-30, 2010

Shewmon, P. (1989), *Diffusion in solids (*2nd ed.) The Minerals, Metals & Materials Society, ISBN 0-87339-105-5, Warrendale, PA, USA

Solmon, H. et al. (1995), Ionic transport properties of yttria-doped zirconia, Solid State Phenomena, Vol. 41, p.103 – 112, ISSN 1012-0394

Vykhodets, V.B. et al. (1987), Oxygen diffusion in α-Ti. II. The calculation of the concentration profile of impurities in the nuclear microanalysis, The Phys. Metal & Metallogr., Vol.64, p.920-923, ISSN 0031-918X

Vykhodets, V.B. et al. (1994), Potential barriers in the migration of tracer oxygen atoms in the $YBa_2Cu_3O_{7-\delta}$ lattice, JETP, Vol.106, N2(8), p.648-662, ISSN 0044-4510

Vykhodets, V. B. et al. (2000), Atomic structure and diffusion properties superanizotropnyh systems, Journal of Solid State Physics, Vol.42, N4, p.595-601, ISSN 0367-3294

Vykhodets, V.B. et al. (2008), Grain Boundary Self-Diffusion of Tracer 18O Atoms in Nanocrystalline Oxide $LaMnO_{3+\delta}$, JETP Letters, Vol. 87, No. 2, pp. 115–119, ISSN 0370-274X

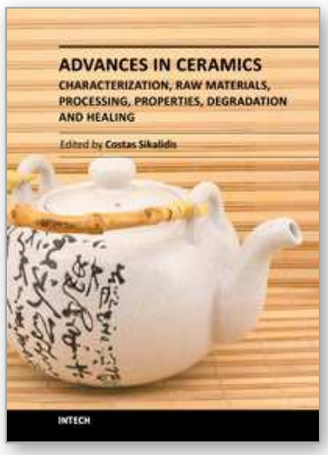

Advances in Ceramics - Characterization, Raw Materials, Processing, Properties, Degradation and Healing
Edited by Prof. Costas Sikalidis

ISBN 978-953-307-504-4
Hard cover, 370 pages
Publisher InTech
Published online 01, August, 2011
Published in print edition August, 2011

The current book consists of eighteen chapters divided into three sections. Section I includes nine topics in characterization techniques and evaluation of advanced ceramics dealing with newly developed photothermal, ultrasonic and ion spattering techniques, the neutron irradiation and the properties of ceramics, the existence of a polytypic multi-structured boron carbide, the oxygen isotope exchange between gases and nanoscale oxides and the evaluation of perovskite structures ceramics for sensors and ultrasonic applications. Section II includes six topics in raw materials, processes and mechanical and other properties of conventional and advanced ceramic materials, dealing with the evaluation of local raw materials and various types and forms of wastes for ceramics production, the effect of production parameters on ceramic properties, the evaluation of dental ceramics through application parameters and the reinforcement of ceramics by fibers. Section III, includes three topics in degradation, aging and healing of ceramic materials, dealing with the effect of granite waste addition on artificial and natural degradation bricks, the effect of aging, micro-voids, and self-healing on mechanical properties of glass ceramics and the crack-healing ability of structural ceramics.

INTECH
open science | open minds

InTech Europe
University Campus STeP Ri
Slavka Krautzeka 83/A
51000 Rijeka, Croatia
Phone: +385 (51) 770 447
Fax: +385 (51) 686 166
www.intechopen.com

InTech China
Unit 405, Office Block, Hotel Equatorial Shanghai
No.65, Yan An Road (West), Shanghai, 200040, China
中国上海市延安西路65号上海国际贵都大饭店办公楼405单元
Phone: +86-21-62489820
Fax: +86-21-62489821

IntechOpen